Near-field microscopy of surface-plasmon polaritons: Localization and internal interface imaging

Sergey I. Bozhevolnyi, Igor I. Smolyaninov,* and Anatoly V. Zayats*
Institute of Physics, University of Aalborg, Pontoppidanstræde 103, DK-9220 Aalborg, Denmark
(Received 21 November 1994)

Using a scanning near-field optical microscope with shear force feedback we directly probe optical fields of surface-plasmon polaritons (SPP's) excited at different interfaces of gold films while simultaneously imaging surface relief structures. We observe that near-field optical images, which are generated due to the SPP propagating along a rough surface, exhibit spatially localized (within ~250 nm) field enhancement by ~5 times, whereas those due to the SPP at a relatively smooth surface show a well-pronounced interference pattern related to the interference between the excited and scattered SPP's. We observe also that near-field optical images ascribed to the SPP excited at an external (gold-air) interface and those due to the SPP at an internal (gold-fluoride) interface exhibit not only some common features but also distinctly different features, which we believe are related to the topography of the internal interface.

I. INTRODUCTION

Surface-plasmon polaritons (SPP's) have been a subject of extensive studies for more than two decades, partly because their inherent surface-localized nature results in an extremely high sensitivity of SPP's to surface properties, such as roughness and absorbate surface coverage.[1] SPP characteristics also contain information about optical properties of media adjacent to the interface, as well as about an interface which can be considered as a transition layer between two media.[2] Since even the most carefully prepared surfaces are not perfectly flat, theoretical and experimental studies of interaction of SPP's with surface roughness represent a significant part of the scientific literature on SPP's. Traditionally, behavior of the SPP at a rough surface has been deduced from (far-field) measurements of light scattered into a free space due to the SPP interaction with surface features.[1,3] Recently developed surface-plasmon microscopy[4] extends the possibilities of far-field measurements, but its lateral resolution is still diffraction limited. This problem can be partially solved by using a photosensitive overlayer to record an interference pattern between the SPP and a reference wave (to analyze the interference pattern, the photoresist layer had to be developed, covered with a metal film, and examined in a scanning electron microscope).[5] However, only with the development of scanning probe techniques did it become possible to study SPP properties virtually at the surface along which the SPP propagates, without surface modification and with the resolution in the nanometer range. It should be stressed that these techniques provide the means for local probing of the SPP field, which knowledge is essential for understanding of various phenomena from scattering of SPP's to surface-enhanced Raman scattering and nonlinear wave interactions involving SPP's.

The first scanning probe technique used for spatially resolved studies of SPP's was the scanning tunneling microscopy (STM) technique.[6–8] In experiments with the STM an additional tunneling current has been observed due to the SPP excitation. However, since there are several effects which might induce the additional current[8] it is difficult to extract SPP field characteristics from the detected signal. A closely related technique, in which the SPP field scattered by a STM tip was detected in the far-field zone, was introduced by Specht *et al.*[9] In another approach,[10] a dielectric SiN probe of an atomic force microscope was used instead of the STM tip. The power of light scattered by a subwavelength-sized scatterer (probe tip) is proportional to the light intensity at the site of the scatterer and, therefore, the signal detected by these two techniques should provide, at least in the first approximation, the SPP local-field intensity. However, there are also some other effects to be taken into account, such as, for example, radiationless energy transfer from the tip to the sample,[9] and the influence of the experimental configuration, especially the detector's position, on the detected signal [this effect has been demonstrated with the inverted photon scanning tunneling microscopy (PSTM) (Ref. 11)]. It is relevant to mention a near-field technique introduced by Fischer and Pohl,[12] in which SPP excitation in small protrusions of an otherwise flat gold film was used to observe single-particle plasmons as well as to image surfaces with protrusions acting as near-field optical probes.

The photon scanning tunneling microscope (PSTM) developed a few years ago[13] makes use of an uncoated fiber tip in order to detect an evanescent field of the light being totally internally reflected at the sample surface. A sharp homogeneous fiber tip immersed in the evanescent optical field can be within certain approximations considered as a detector of the square modulus of the electric near field.[14] Therefore, contrary to the aforementioned techniques, the PSTM enables one to measure directly the SPP local field near the studied surface.[15] Interesting observations of SPP behavior in fractals have recently

0163-1829/95/51(24)/17916(9)/$06.00

been reported by Tsai *et al.*[16] In this work the PSTM with optical feedback was used, i.e., the detected optical signal was kept constant when scanning the fiber tip along the surface. However, in order to extract useful information from such measurements the surface topography has to be determined simultaneously with near-field optical measurements. For such a purpose one can use a shear force technique,[17,18] in which a vibration amplitude of the fiber tip provides the signal for a feedback system, and the tip-surface distance can be maintained in the same way as in a conventional atomic force microscope.

Here we present results of an experimental study of SPP's carried out by using the PSTM combined with shear force regulation of the tip-surface distance. Near-field optical images generated due to SPP's excited at different interfaces of gold films are obtained simultaneously with topographical images of these films. We observe spatially localized enhancement of the SPP field intensity at a rough surface. We also obtain near-field optical images, which are generated due to the SPP propagating along the inner interface of the sample recently studied with the STM technique,[19] and recognize some features in these images as being related to the topography of the internal interface.

II. EXPERIMENTAL ARRANGEMENT

The optical part of our experimental setup is shown schematically in Fig. 1. The setup consists of the PSTM,[13] combined with a shear force based feedback system[18] and an arrangement for SPP excitation in the usual Kretschmann configuration.[20] The light from a He-Ne laser ($\lambda \approx 633$ nm, $P \approx 3$ mW) is used for the SPP excitation. The laser beam is polarized parallel to the plane of incidence (p polarization), intensity modulated by an acousto-optic modulator (modulation frequency ~ 20 kHz), and focused onto the base of a prism with a gold film (focal length ≈ 500 mm, spot size ~ 400 μm). The reflected light is detected by a photodiode, and the excitation of the SPP is recognized as a minimum in the angular dependence of the reflected light power (attenuated total reflection minimum).[1]

The SPP local field is probed with a sharp fiber tip, which is fabricated by etching of a single-mode silica fiber in a 40% solution of hydrofluoric acid during a time period of 55 min.[21] Another end of the fiber is optically coupled to a photomultiplier tube, whose signal at the modulation frequency is synchronously detected by using a lock-in amplifier. The position of the fiber tip is controlled by a three-coordinate piezotranslator based on bimorphs. The fiber tip can be scanned over the sample surface with a constant tip-surface distance (~ 5 nm) by using the shear force feedback described in detail elsewhere.[22] The main idea is to keep a vibration amplitude of the fiber tip at some level, which is below the amplitude level for the tip being far from the sample surface. In our experiment the amplitude (1–10 nm) of tip resonant vibrations (frequency ≈ 8 kHz) is measured by using synchronous detection (at the vibration frequency) of light diffracted from a laser beam after passing through the fiber perpendicular to its axis (Fig. 1). Therefore, a surface topography can be imaged with a resolution on the nanometer scale, while recording simultaneously a near-field optical image corresponding to a distribution of the SPP local-field intensity near the film surface. It should be mentioned that a typical recording time of the 4×4-μm^2 surface area is ≈ 20 min, and a temporal drift of the piezotranslator with respect to the sample is less than 3 nm/min, so the drift can be regarded as negligibly small. Note that the scan speed, which can otherwise be up to 5 μm/s, is limited by the integration time of 100 ms needed to ensure a sufficiently high signal-to-noise ratio in the detected optical signal (0.01–1 nW).

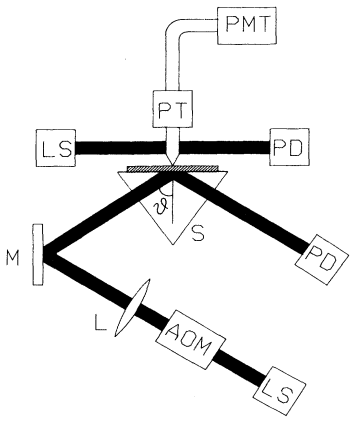

FIG. 1. Experimental setup for studying surface polaritons with a photon scanning tunneling microscope. LS, laser source; AOM, accousto-optic modulator; L, lens; M, mirror; S, sample; PD, photodiode; PT, piezoelectric translator; and PMT, photomultiplier tube. The polarization of the light is parallel to the figure plane.

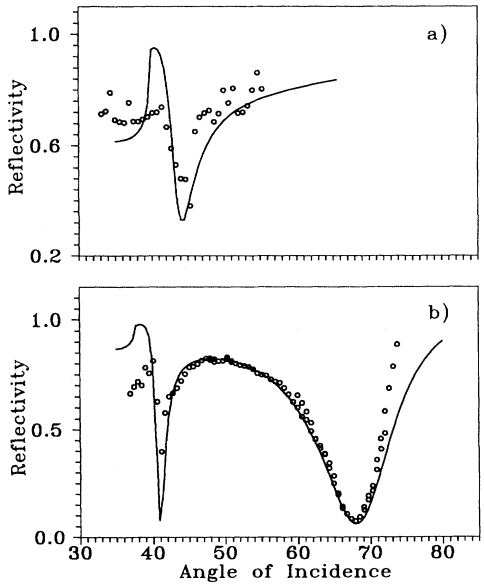

FIG. 2. Angular excitation spectra of surface polaritons measured (circles) and calculated (solid lines) for the one-layer (a) and two-layer (b) structures, respectively.

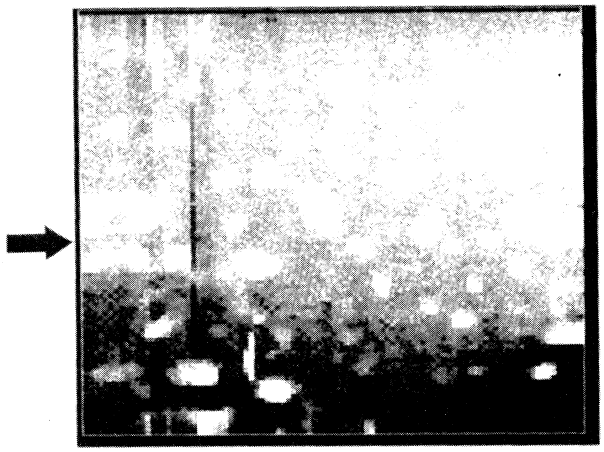

(a)

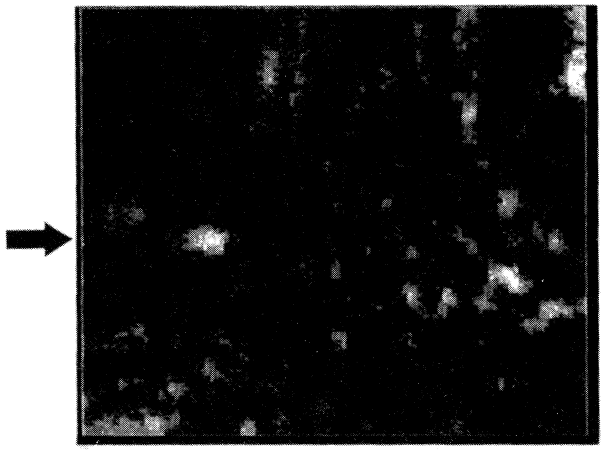

(b)

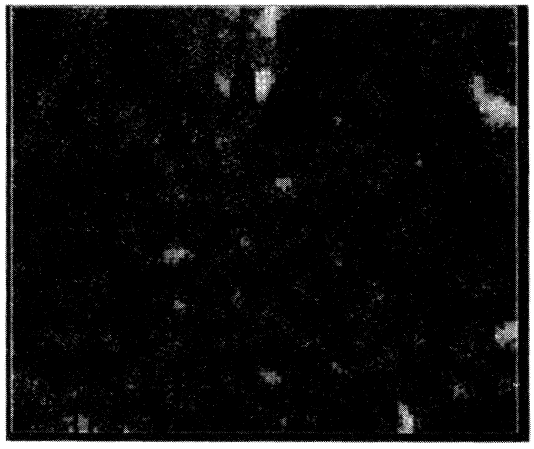

(c)

FIG. 3. Gray-scale topographical (a) and near-field optical (b) and (c) images of 4×4 μm^2 obtained with the one-layer structure. The maximum depth of the topographical image is 40 nm. The optical images were taken at the same place with the polariton being resonantly excited (b), and with a $\approx 3°$ deviation of the angle of incidence from the resonance one (c). The optical images are presented in the common scale corresponding to $\sim 0-30$ pW of the detected optical signal. Arrows indicate the directions of the cross sections shown in Fig. 4.

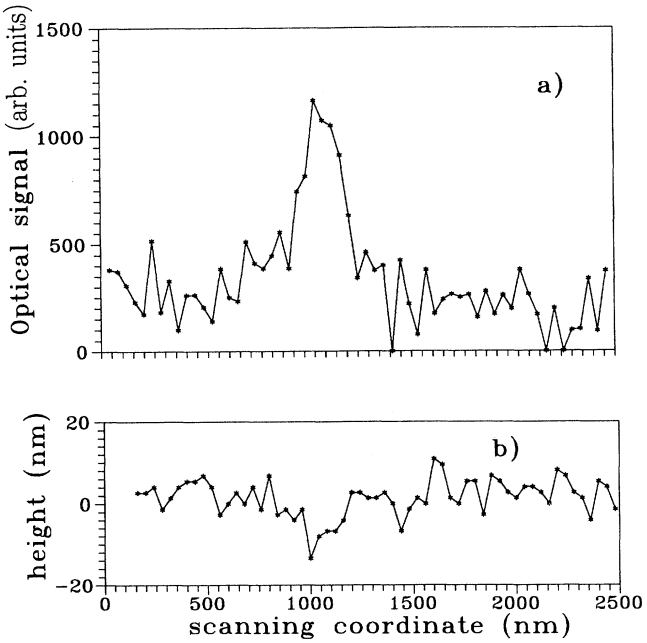

FIG. 4. The distribution of the near-field optical signal (a) and the appropriate surface profile (b) obtained from the images shown in Fig. 3 along the directions indicated by the arrows.

III. EXPERIMENTAL RESULTS

We studied two structures, namely a gold film (thickness ≈ 80 nm) evaporated on a glass prism with the refractive index $n = 1.56$, and a two-layer structure consisting of a gold film (thickness ≈ 60 nm) deposited on a magnesium fluoride layer (thickness ≈ 170 nm, $n = 1.28$) placed on the top of a prism ($n = 1.64$). The first structure allows us to excite the SPP at the gold-air interface, whereas the second one gives us the possibility to excite two SPP modes, i.e, a fast SPP (FSPP) at the gold-air interface and a slow SPP (SSPP) at the gold-fluoride (internal) interface.[19] Angular dependences of the reflected light power were measured for both structures in order to determine the excitation angles for these SPP's (Fig. 2). The excitation of the relevant SPP results in a pronounced minimum in the angular dependence of the reflectivity of p-polarized light. By fitting the experimen-

tally obtained angular dependences to those calculated for the appropriate layered structures, the dielectric constants of the gold films have been found to be $n_1 \approx 0.13 + 2.7i$ and $n_2 \approx 0.13 + 2.75i$ in the first and second structures, respectively. Using these data together with the values of excitation angles, one can determine (assuming perfectly flat and sharp interfaces) various characteristics of the appropriate SPP, such as the effective wavelength, the propagation length, and the penetration depths in neighbor media.

The SPP field intensity distributions near the surfaces of these samples were studied by using the PSTM to obtain near-field optical images while simultaneously imaging the surface profiles with the shear force technique. It should be noted that all images presented here are oriented in the way that the SPP if excited propagates upwards in the vertical direction.

A. One-layer structure (localization of the SPP)

Topographical images of the gold film surface of the first sample showed the typical island structure of the film consisting of bumps (pits) with various heights (5–100 nm) and sizes (50–1000 nm) in the surface plane [Fig. 3(a)]. The optical signal from the SPP being resonantly excited [$\theta \approx 45°$, cf. Fig. 2(a)] was ~ 10 pW on average, but optical images also exhibited some rather bright spots [Fig. 3(b)]. Typically, such a spot had a size of ~ 250 nm, and the peak signal in it was up to five times larger than the average level (Fig. 4). If the angle θ of incidence was out of resonance by a few degrees then the

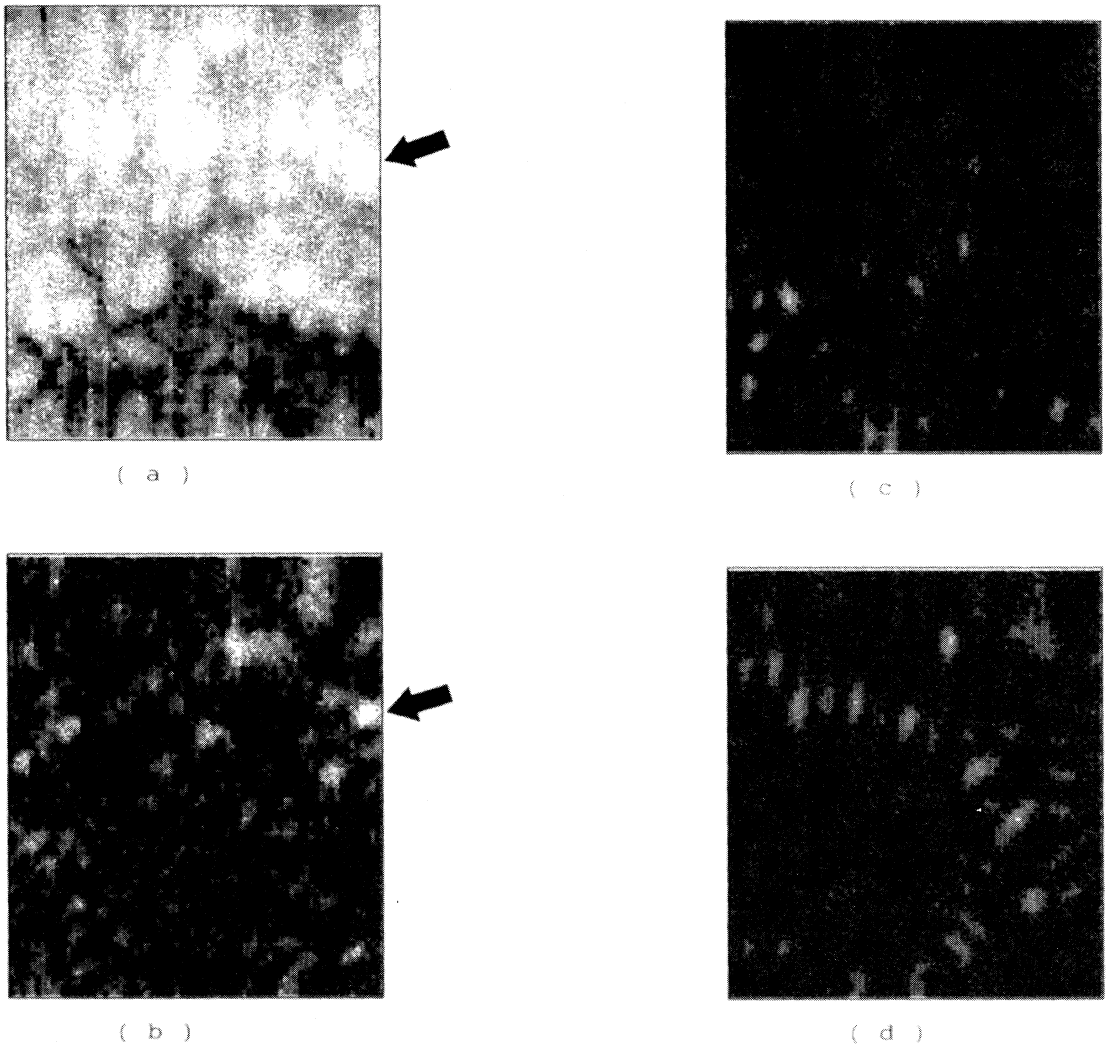

FIG. 5. Gray-scale topographical (a) and near-field (b) and far-field optical (c) and (d) images of 3×3.5 μm^2 obtained with the one-layer structure. The maximum depth of the topographical image is 45 nm. The optical images were taken at the same place (with the polariton being resonantly excited) for different tip-surface distances: ~ 5 nm (b), 3 μm (c), and 30 μm (d). The optical images are presented in the common scale corresponding to ~ 2–30 pW of the detected optical signal. Arrows indicate the bright spot (b) and its position (a).

average optical signal was half as much, the bright spots seen at resonance disappeared, but some spots, though not so bright, came up at other places [compare Figs. 3(b) and 3(c)]. In general, similar weak spots (the signal enhancement factor ~ 3) were observed at various excitation angles different from the resonant one. The dependence of optical images on the tip-surface distance was also studied. It appeared that after moving the fiber tip ~ 1 μm away from the surface the average optical signal decreased about by half, and then was nearly independent on the tip-surface separation, whereas the bright spots were present only on the near-field images (Fig. 5). Finally, one can notice that the observed bright spots are almost round, and that their locations are not correlated with the local surface profiles: the peak signal can correspond to the surface pit (Fig. 4) or to the surface bump (Fig. 5). We have also found that the bright spots can be observed at some intermediate positions of the surface slope. But the most important circumstance, in this context, is that bright spots are not seen at places with (nearly) the same topography as that of the places they are present at (Figs. 3 and 5).

The angular and tip-surface distance dependences of optical images indicate a strong interaction of the SPP with surface roughness, which results in the circumstance that, on average, only a half of the optical signal measured (for resonance excitation) near the surface is related to the SPP field intensity. Another part is likely to be due to the propagating (in air) components of light scattered by surface roughness. This part should not be much dependent on either the tip-surface distance or the angle of incidence. Actually, only the observed bright spots are directly related to the SPP excitation. We believe that the presence of these spots can be regarded as evidence of strong localization of the SPP caused by surface roughness.

Localization of light can occur in media with strong disorder, so that the interference of multiple-scattered light makes propagation of light impossible, leading instead to localization.[23] Localization of the SPP (parallel to the metal surface) can be caused accordingly by surface roughness.[24] Since the size of the observed bright spots is at most half that of the SPP wavelength (~ 570 nm), the Ioffe-Regel criterium for localization is practically satisfied. The shape of the spots and the absence of correlation between locations of the spots and the local surface profiles also support our hypothesis of the SPP localization in the structure we studied. The angular dependence of optical images is more difficult to interpret. It seems evident that the SPP localization should also be seen at other (than the resonant) excitation angles, since phase matching is not that important for excitation of localized SPP's. On the other hand, the SPP localization is an essentially two-dimensional phenomenon related to the multiple scattering of SPP's in the surface plane. Therefore, if the efficiency of the scattering of the incident (out of resonance) beam into propagating SPP's is less than the combined efficiency of the resonant SPP excitation with the subsequent SPP scattering in the surface plane, then the SPP localization should be most pronounced at resonance. We believe that this can be a reason for the absence of bright spots out of resonance [the SPP excitation at resonance is rather efficient; see Fig. 2(a)]. Moreover, in such a case the aforementioned weak spots observed out of resonance might also be related to the SPP localization.

As far as recently published results on the SPP behavior in fractals[16] are concerned, we would like to stress that PSTM images obtained in Ref. 16 with optical feedback (constant intensity mode) can be rather misleading because of the strong influence of waves propagating in air and generated due to the scattering of evanescent waves by surface roughness.[25] For example, a 50-nm-high step on the silica surface can result in images with giant corrugations with up to 300-nm height depending on the preset value for the optical feedback.[26] Therefore, without knowledge of the surface topography one can hardly separate the contribution (in the detected signal) of light scattered into a free space by macroscopic surface features and the contribution stemming from the spatially localized (in the surface plane) light-induced dipole modes.[27]

The near-field optical images presented here, contrary to those from Ref. 16, have been obtained with a constant tip-surface distance (~ 5 nm), and the contribution of propagating (in air) waves in the detected optical signal is known from angular and distance dependences of optical images (~ 5 pW on average). This contribution is about five times less than the peak signal values at bright spots. The propagating waves cannot form a spot image with a size less than the diffraction limit ($\lambda/2 \approx 316$ nm). One can presume that the actual spot size is even less than 250 nm due to the limited resolution of the PSTM. Therefore, the observed spatially localized signal enhancement (bright spots) is indeed related to the SPP (near) field enhancement and can be regarded as the evidence of the SPP localization. Finally, we would like to point out that

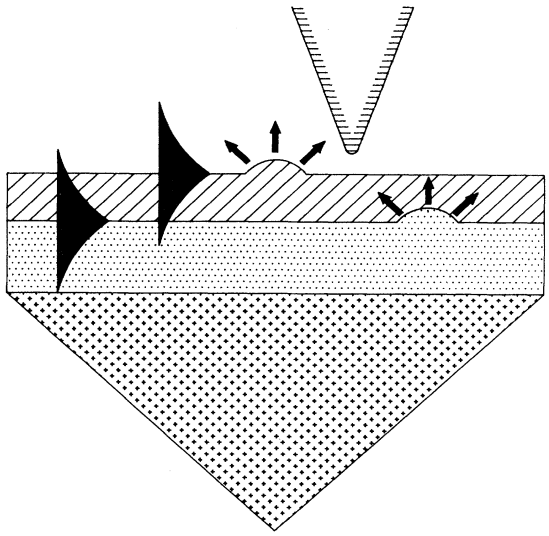

FIG. 6. Schematic representation of the interactions of the fast and slow polaritons with the surface features at the external and internal interfaces. The optical fiber tip of a near-field microscope used to probe the polariton field is also shown.

(a)

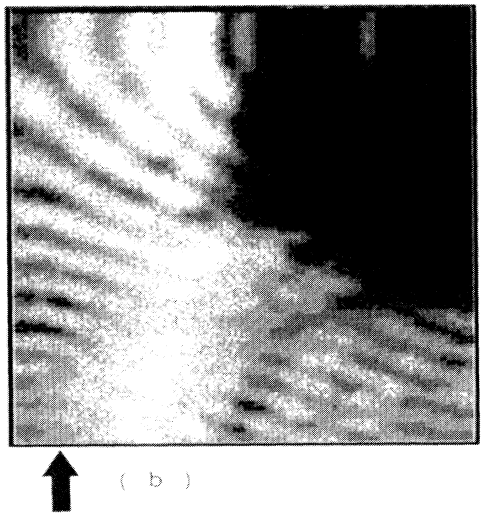

(b)

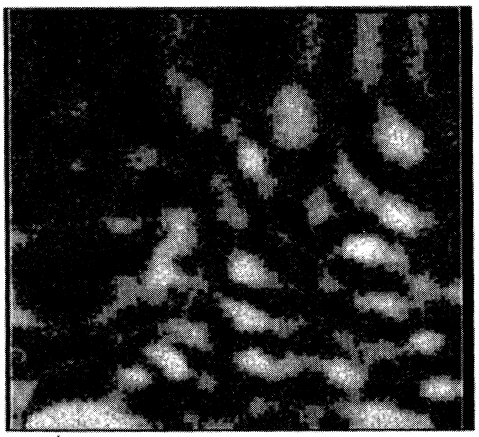

(c)

a surface with random roughness, which is very often the case, can also be considered as an example of a fractal (in the surface plane) structure, which makes the objects studied here and in Ref. 16 similar to each other. We think that localization of plasmons could have taken place under conditions described in Ref. 16, but the experimental evidence presented there is indirect and far from being conclusive.

B. Two-layer structure (internal interface imaging)

The second sample consisting of a two-layer structure allows us to excite two SPP modes (the FSPP at the gold-air interface and the SSPP at the gold-fluoride interface) by appropriately adjusting the angle θ of incidence [cf. Fig. 2(b)]. The idea of our experiment is schematically represented in Fig. 6. If the gold film is not too thick, the fiber tip can probe both the FSPP and SSPP fields, either of which is most sensitive to the topography of the appropriate interface. Recording three images at the same place—the topographical image of the external interface with the shear force technique, and two near-field optical images generated in turn due to two SPP modes—gives in principle the possibility to deduce the topography of the internal interface. Though this is not an easy problem, one can presume that the reconstruction of the internal surface relief might be performed at least for two extreme cases: for slowly varying (adiabatic) surface profiles, and for subwavelength features (similar to pointlike scatterers) placed far away from each other. In the first case the SPP scattering can be neglected, and the detected optical signal due to the SSPP (propagating along the internal interface) is more or less directly related to the local film thickness. In the second case coupling between scatterers can be disregarded, and the power and phase of the scattered light is connected to the size and sign (bump or pit) of the scatterer. In both cases after some calibration procedure the reconstruction of the internal interface seems feasible.

We calculated the ratio R between the maximum value of the SPP field (at the interface) and the value of this field at another interface as being equal to $R \sim 6$ for both SPP's. This value of R is large enough to detect the optical signal from the SSPP, but sufficiently small to decrease the influence of the surface profile of one interface on the SPP at another one. Topographical images of the gold film surface showed that the external interface is more smooth than that of the first structure (the average surface variation is ~ 10 nm), but it has rarely spaced micron-sized bumps with 100–200-nm heights. Conse-

FIG. 7. Gray-scale topographical (a) and near-field (b) and far-field optical (c) images of 3.5×4 μm^2 obtained with the two-layer structure. The maximum depth of the topographical image is 140 nm. The optical images were taken at the same place (with the fast polariton being resonantly excited) for different tip-surface distances: ~ 5 nm (b) and 12 μm (c). The optical images are presented in different scales corresponding to ~ 10–600 pW (b) and ~ 0–20 pW (c) of the detected optical signal. Arrows indicate the directions of the cross sections shown in Fig. 8.

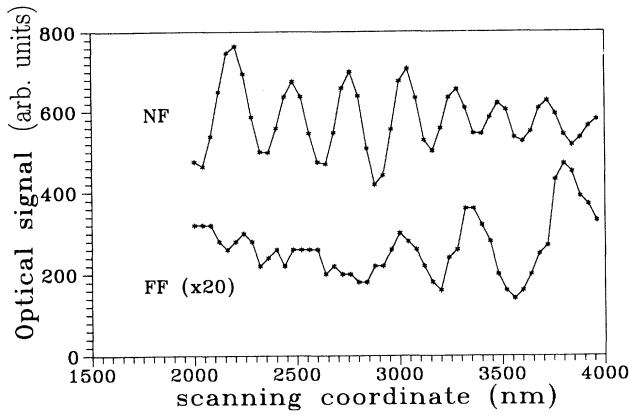

FIG. 8. The cross sections of the near-field (NF) and far-field (FF) optical images from Fig. 7 along the directions indicated by the arrows.

quently, the detected optical signal due to the FSPP was on average about 30 times higher than the one due to the SPP of the first sample, and the appropriate near-field optical images usually exhibited a well-pronounced interference pattern related to the interference between the excited and scattered FSPP's (Fig. 7). The angular and distance dependences of the optical signal in this case were also quite different from those observed for the first sample. The average optical signal was about 20 times smaller if the angle of incidence was out of resonance by $\sim 2°$ or if the tip was moved $\sim 1\ \mu$m away from the surface. It is interesting to note that the far-field optical images also showed an interference pattern [Fig. 7(c)], but its period was considerably larger, corresponding to the wavelength of waves propagating in air (Fig. 8).

The interference pattern related to the FSPP [Fig. 7(b)] can be used to determine directly the FSPP wavelength. Taking into account the propagation direction of the FSPP (SPP's propagate upwards for all images), the nonlinearity of the image related to a nonlinear response of the piezotranslator, and the period of the interference pattern (Fig. 8), we estimated the FSPP wavelength as being equal to $\Lambda_e \sim 550$ nm, whereas the value calculated from the angle θ of the resonance FSPP excitation [Fig. 2(b)] is $\Lambda_t \sim 590$ nm. We think that the accuracy of direct evaluation of the SPP wavelength from the interference pattern is dependent mainly on the accuracy of the image linearization. It is clear that such an interference pattern can also be used in order to determine the relative amplitude and phase of the SPP scattered by the surface inhomogeneity. Actually, surface features can be specifically designed in order to realize and to study (by using this approach) various optical configurations in two dimensions, such as apertures, lenses, resonators, etc.

Several different places of the sample surface were studied in order to examine the approach suggested for the internal interface imaging. Two near-field optical images generated in turn due to two SPP modes approximately at the same place as previously (Fig. 7) are shown in Fig. 9. The average optical signal detected from the SSPP (propagating along the internal gold-fluoride interface) was about 20 times smaller than that from the FSPP, which agrees with our estimations of R (one should take into account the difference in the excitation efficiency, and that the signal is related to the field intensity, i.e., to R^2). The surface bump [Fig. 7(a)] is apparently present at both interfaces since it gives rise to the scattering of both SPP's, resulting in turn in the interference patterns on both images (Fig. 9). The periods of these patterns are distinctly different (Fig. 10), as it should be due to the difference in the wavelengths of SPP's: $\Lambda_f \sim 590$ nm (FSPP) and $\Lambda_s \sim 420$ nm (SSPP). Judging from the distribution of the detected signal in the image generated due to the SSPP [Fig. 9(b)], one may

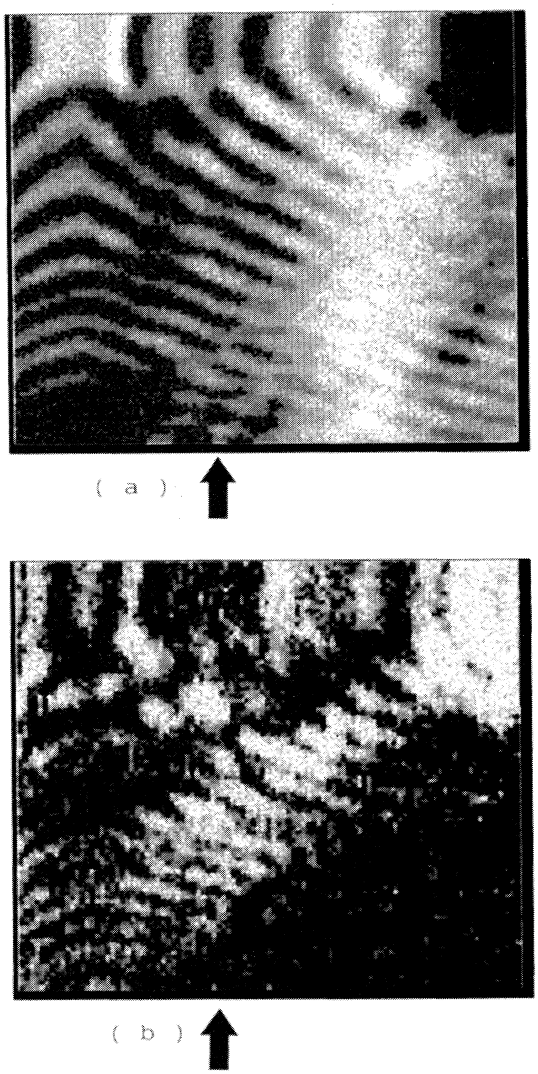

FIG. 9. Near-field optical images of $4\times4\ \mu m^2$ taken at nearly the same place as those in Fig. 7, and generated due to the fast (a) and slow (b) polaritons being resonantly excited in turn. The optical images are presented in different scales corresponding to ~ 10–600 pW (a) and ~ 0–30 pW (b) of the detected optical signal. Arrows indicate the directions of the cross sections shown in Fig. 10.

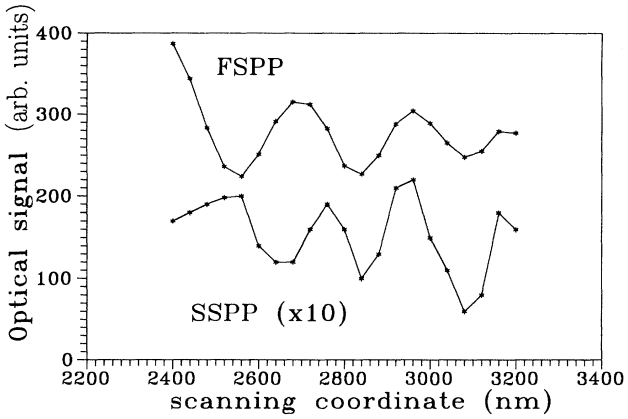

FIG. 10. The cross sections of the near-field optical images, which were generated in turn due to the fast (FSPP) and slow (SSPP) polaritons, from Fig. 9 along the directions indicated by the arrows.

presume that the gold film is relatively thick at the area corresponding to the lower right corner of the image, and thin at the bump area (upper right corner). The appropriate images recorded at another place on the sample reveal a relatively small bump at the external interface, whose area and height are $\sim 0.6 \times 0.6\ \mu m^2$ and 100 nm, respectively [Fig. 11(a)]. This bump results in FSPP scattering, leading in turn to the interference pattern [Fig. 11(b)], which is quite similar to the previously observed one [Fig. 9(a)]. However, it seems that in this case the FSPP propagates along the bump surface and scatters on the bump borders, thus forming a compact standing-wave field distribution at the bump surface [the upper left corner in Fig. 11(b)]. This can serve, at least in the first approximation, as an example of a microresonator (microcavity) for the SPP's. The SSPP propagation along the internal interface was not much influenced by this bump, but the appropriate optical image [Fig. 11(c)] shows more than a tenfold increase of the detected signal at the other place, which does not exhibit any specific features either in the external interface topography or in the optical image generated due to the FSPP (the lower right corner in Fig. 11). One may reasonably assume that there is a strong scatterer at the internal interface and that it is probably a pit (not bump), otherwise it would also have strongly affected the FSPP propagation along the external interface. However, it is clear that in order to be more conclusive one has to study, first, images obtained with structures which have specific and known features present on both interfaces.

IV. CONCLUSIONS

Using the PSTM with the shear force feedback we have directly probed optical fields of SPP's excited at different interfaces of gold films, while simultaneously recording appropriate surface profiles. We have demonstrated that the experimental technique developed is capable of providing not only high-quality and high-resolution near-

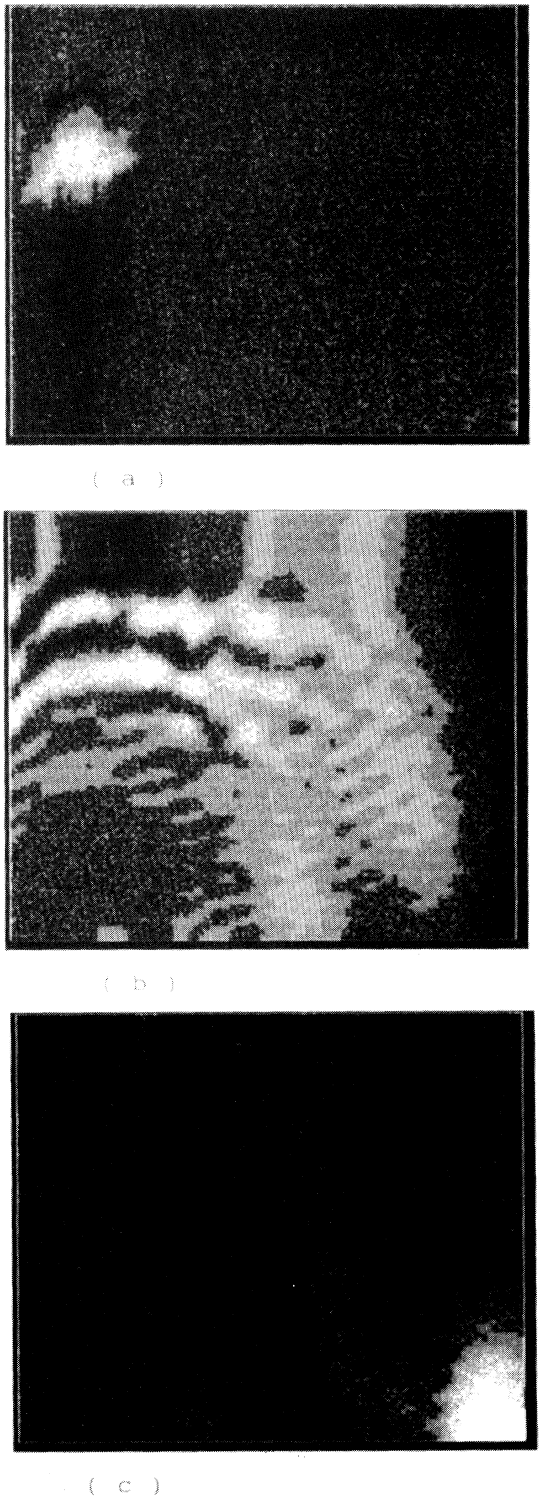

FIG. 11. Gray-scale topographical (a) and near-field optical (b) and (c) images of $4 \times 4\ \mu m^2$ obtained with the two-layer structure. The maximum depth of the topographical image is 115 nm. The optical images were taken at the same place with the fast (b) and slow (c) polaritons being resonantly excited in turn. The optical images are presented in the different scales corresponding to ~ 20–500 pW (b) and ~ 0–50 pW (c) of the detected optical signal.

field optical images generated due to the SPP's but also, at the same time, adequate topographical images, without which the interpretation of optical images is hardly possible. Note that, except for some topographical images in which an average linear slope has been subtracted, the presented images are unprocessed.

The SPP excited at the surface of the gold film with a typical island structure has been studied. It has been found that the near-field optical images exhibit a spatially localized enhancement of the SPP field intensity in the form of ~250-nm-sized bright spots. The enhancement ratio (~5), size, and round shape of the spots, and angular and distance dependences of the optical images, can be regarded together, in our opinion, as evidence of the strong localization of the SPP in the structure we studied. However, SPP behavior at excitation angles different from the resonant one has yet to be understood in order to elucidate the situation with SPP localization in this case.

We have studied the two-layer structure, which supports propagation of two SPP modes: the FSPP along the external (gold-air) interface, and the SSPP along the internal (gold-fluoride) interface. When exciting the FSPP we have observed well-pronounced interference patterns formed due to the interference between excited and scattered FSPP's. These interference patterns have been suggested for use, in general, in studying various phenomena in two-dimensional optics and, in particular, for direct measurements of the SPP wavelength. We have discussed the possibility of internal interface reconstruction by using a topographical image of the external interface and two near-field optical images generated in turn due to the FSPP and SSPP propagating along the external and internal interfaces, accordingly. We have observed that these optical images not only exhibit some common but also distinctly different features, which can be related to the topography of the internal interface. The results obtained demonstrate that in some cases the internal interface imaging is feasible by using the developed approach, but a systemic study of this technique should be carried out by imaging specially fabricated samples with various known structures at both interfaces. The appropriate theoretical consideration of the imaging properties of the PSTM in such a configuration is also desirable.

ACKNOWLEDGMENTS

The authors are grateful to Dr. T. Skettrup (Denmark Technical University) for providing the two-layer structure used in our experiments, and to Professor O. Keller (Aalborg University) for useful discussions.

*On leave from Institute of Spectroscopy, Russian Academy of Sciences, 142092 Troitsk, Russia.

[1]H. Raether, *Surface Plasmons,* Springer Tracts in Modern Physics Vol. 111 (Springer, Berlin, 1988).

[2]V. M. Agranovich, in *Surface Polaritons,* edited by V. M. Agranovich and D. L. Mills (North-Holland, Amsterdam, 1982), p. 187.

[3]A. A. Maradudin, in *Surface Polaritons* (Ref. 2), p. 405.

[4]E. Yeatman and E. A. Ash, Electron. Lett. **23**, 1091 (1987); B. Rothenhäusler and W. Knoll, Nature (London) **332**, 615 (1988).

[5]F. Keilmann, Proc. SPIE **1029**, 50 (1988).

[6]R. Möller *et al.*, J. Vac. Sci. Technol. B **9**, 506 (1991).

[7]N. Kroo *et al.*, Europhys. Lett. **15**, 289 (1991).

[8]C. Baur *et al.*, in *Near Field Optics,* edited by D. W. Pohl and D. Courjon (Kluwer, The Netherlands, 1993), p. 325.

[9]M. Specht *et al.*, Phys. Rev. Lett. **68**, 476 (1992).

[10]R. B. G. de Hollander, N. F. van Hulst, and R. P. H. Kooyman, Ultramicroscopy (to be published).

[11]B. Hecht, H. Heinzelman, and D. W. Pohl, Ultramicroscopy (to be published).

[12]U. Ch. Fischer and D. W. Pohl, Phys. Rev. Lett. **62**, 458 (1989).

[13]R. C. Reddick, R. J. Warmack, and T. L. Ferrel, Phys. Rev. B **39**, 767 (1989); D. Courjon, K. Sarayeddine, and M. Spajer, Opt. Commun. **71**, 23 (1989); F. de Fornel *et al.*, Proc. SPIE **1139**, 77 (1989).

[14]D. Van Labeke and D. Barchiesi, J. Opt. Soc. Am. A **10**, 2193 (1993).

[15]O. Marti *et al.*, Opt. Commun. **96**, 225 (1993); H. Bielefeldt *et al.*, in *Near Field Optics* (Ref. 8), p. 281; P. M. Adam *et al.*, Phys. Rev. B **48**, 2680 (1993); P. Dawson, F. de Fornel, and J. P. Goudonnet, Phys. Rev. Lett. **72**, 2927 (1994).

[16]D. P. Tsai *et al.*, Phys. Rev. Lett. **72**, 4149 (1994).

[17]E. Betzig, P. L. Finn, and J. S. Weiner, Appl. Phys. Lett. **60**, 2484 (1992); R. Toledo-Crow *et al.*, *ibid.* **60**, 2957 (1992).

[18]A. Schchemelin *et al.*, Rev. Sci. Instrum. **64**, 3538 (1993).

[19]I. Smolyaninov, A. Zayats, and O. Keller, Phys. Lett. A (to be published).

[20]E. Kretschmann, Z. Phys. **241**, 313 (1971).

[21]S. I. Bozhevolnyi, O. Keller, and M. Xiao, Appl. Opt. **32**, 4864 (1993).

[22]S. I. Bozhevolnyi, I. I. Smolyaninov, and O. Keller, Appl. Opt. (to be published).

[23]S. John, Phys. Rev. Lett. **58**, 2486 (1987); H. De Raedt, Ad Lagendijk, and P. de Vries, *ibid.* **62**, 47 (1989).

[24]K. Arya, Z. B. Su, and J. L. Birman, Phys. Rev. Lett. **54**, 1559 (1985).

[25]N. F. van Hulst *et al.*, Ultramicroscopy **42-44**, 416 (1992); N. F. van Hulst, F. B. Segerink, and B. Bölger, Opt. Commun. **87**, 212 (1992).

[26]F. de Fornel *et al.*, in *Near Field Optics* (Ref. 8), p. 59.

[27]Strictly speaking, the propagating waves scattered into a free space and the confined SPP fields can be treated as separate only in the absence of a probe tip. In the presence of the tip, such a distinction is an approximation, which is valid as long as the field perturbation by the tip is sufficiently small. This approximation is generally accepted and, to a large extent, justified for the PSTM with an uncoated fiber tip (see Refs. 13–15, 25, and 26).

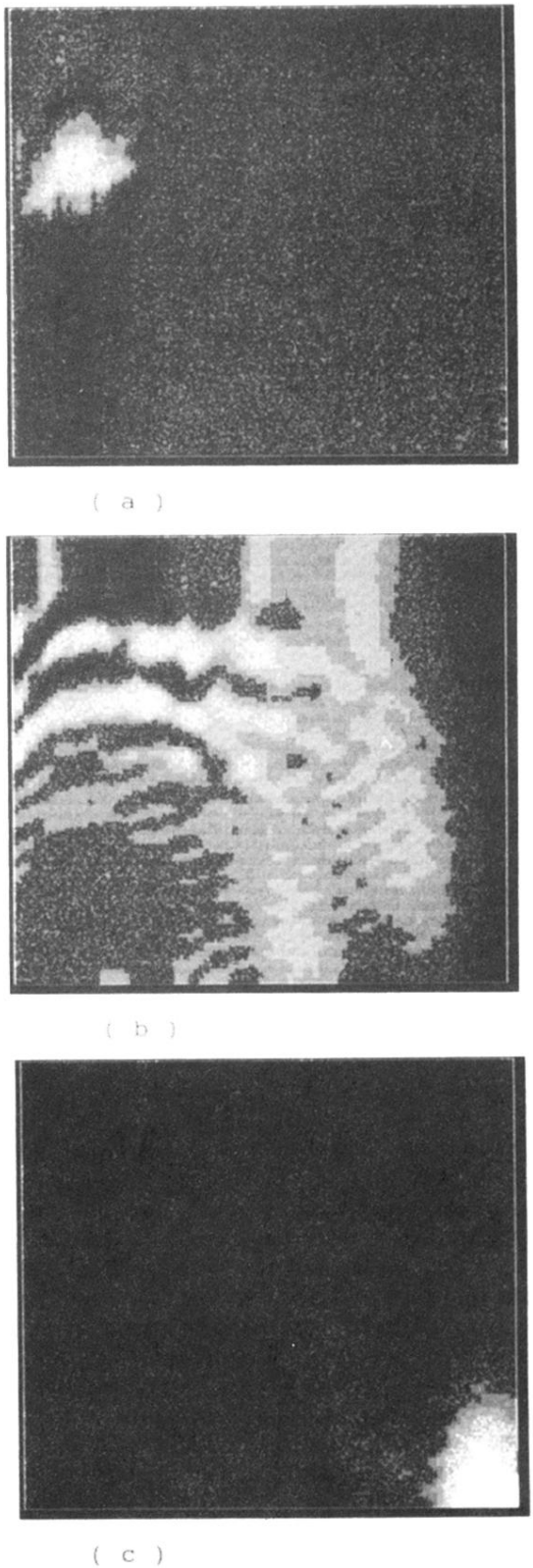

FIG. 11. Gray-scale topographical (a) and near-field optical (b) and (c) images of 4×4 μm^2 obtained with the two-layer structure. The maximum depth of the topographical image is 115 nm. The optical images were taken at the same place with the fast (b) and slow (c) polaritons being resonantly excited in turn. The optical images are presented in the different scales corresponding to $\sim$20–500 pW (b) and $\sim$0–50 pW (c) of the detected optical signal.

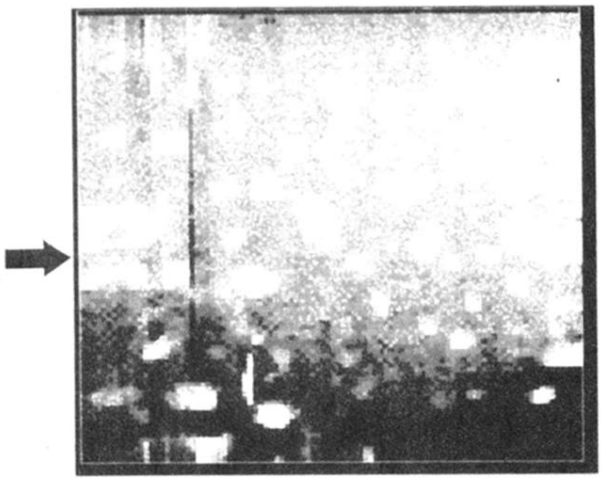

(a)

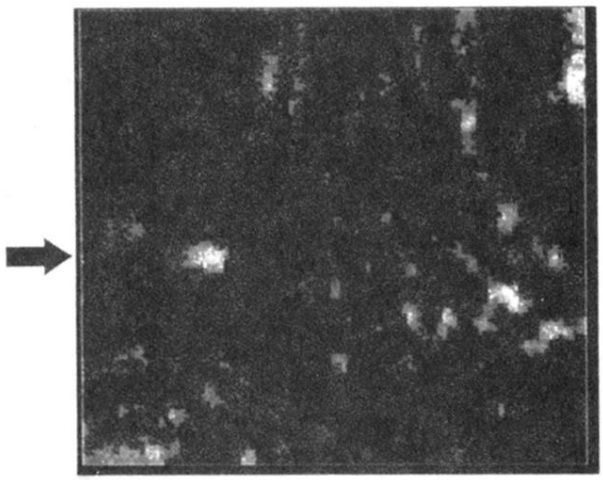

(b)

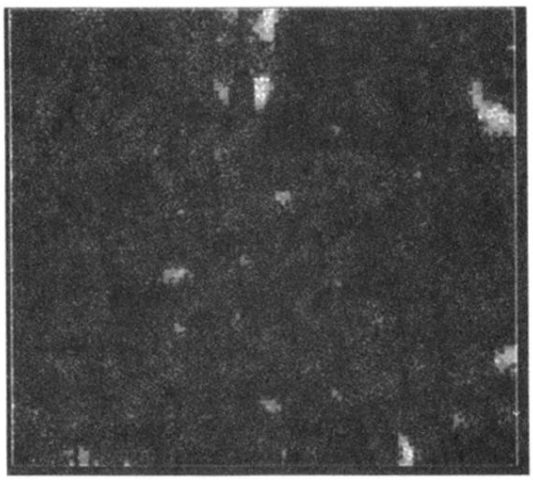

(c)

FIG. 3. Gray-scale topographical (a) and near-field optical (b) and (c) images of 4×4 μm^2 obtained with the one-layer structure. The maximum depth of the topographical image is 40 nm. The optical images were taken at the same place with the polariton being resonantly excited (b), and with a $\approx3°$ deviation of the angle of incidence from the resonance one (c). The optical images are presented in the common scale corresponding to $\sim$0–30 pW of the detected optical signal. Arrows indicate the directions of the cross sections shown in Fig. 4.

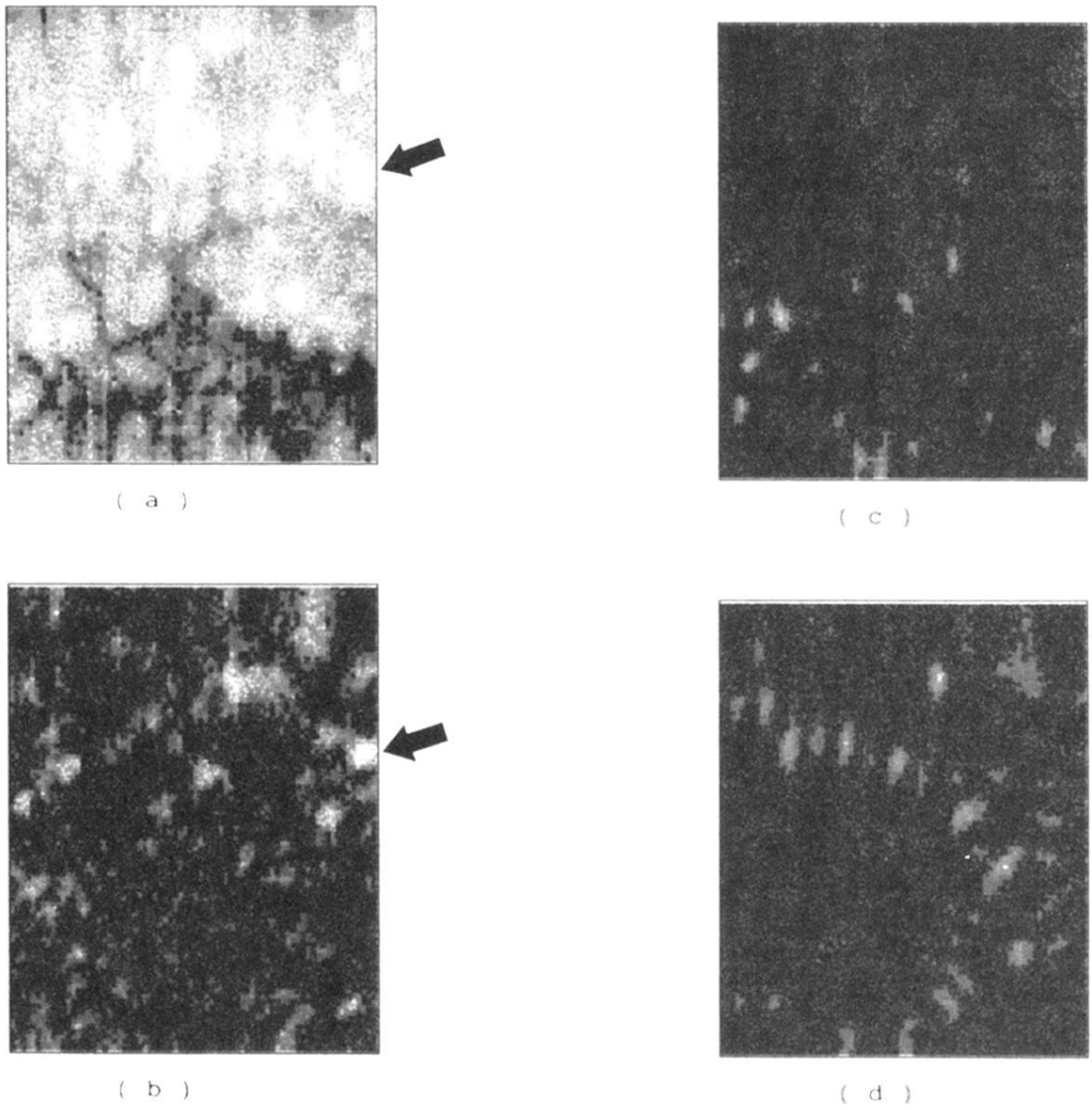

FIG. 5. Gray-scale topographical (a) and near-field (b) and far-field optical (c) and (d) images of $3\times3.5\ \mu m^2$ obtained with the one-layer structure. The maximum depth of the topographical image is 45 nm. The optical images were taken at the same place (with the polariton being resonantly excited) for different tip-surface distances: ~5 nm (b), 3 μm (c), and 30 μm (d). The optical images are presented in the common scale corresponding to ~2–30 pW of the detected optical signal. Arrows indicate the bright spot (b) and its position (a).

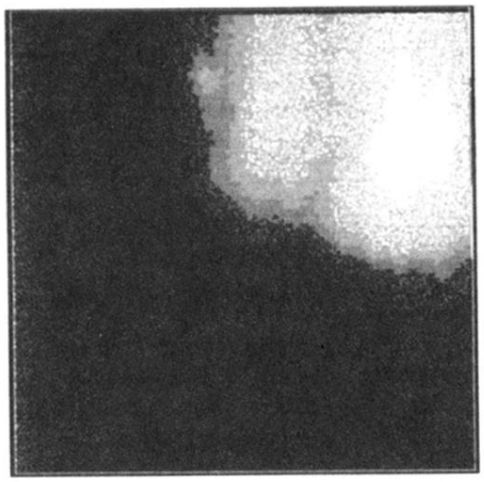

(a)

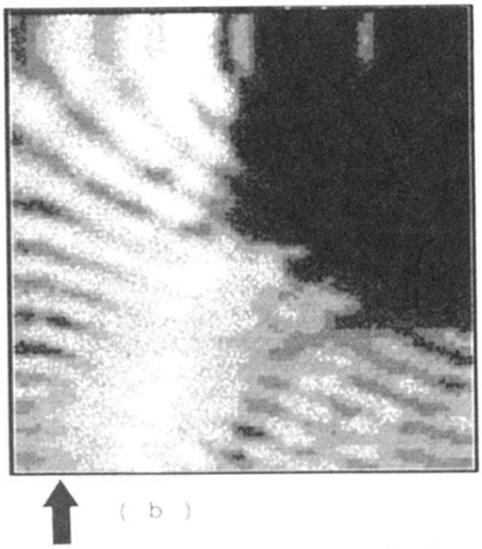

(b)

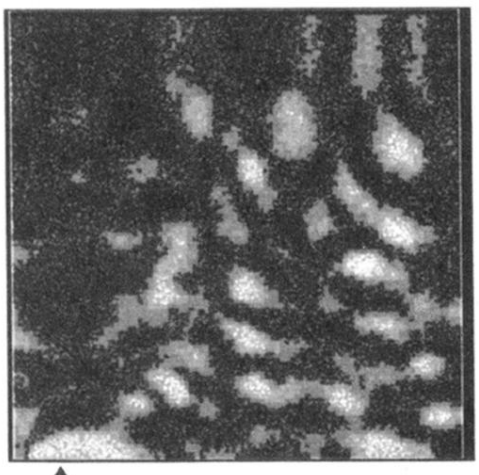

(c)

FIG. 7. Gray-scale topographical (a) and near-field (b) and far-field optical (c) images of 3.5×4 μm^2 obtained with the two-layer structure. The maximum depth of the topographical image is 140 nm. The optical images were taken at the same place (with the fast polariton being resonantly excited) for different tip-surface distances: ~5 nm (b) and 12 μm (c). The optical images are presented in different scales corresponding to $\sim10-600$ pW (b) and $\sim0-20$ pW (c) of the detected optical signal. Arrows indicate the directions of the cross sections shown in Fig. 8.

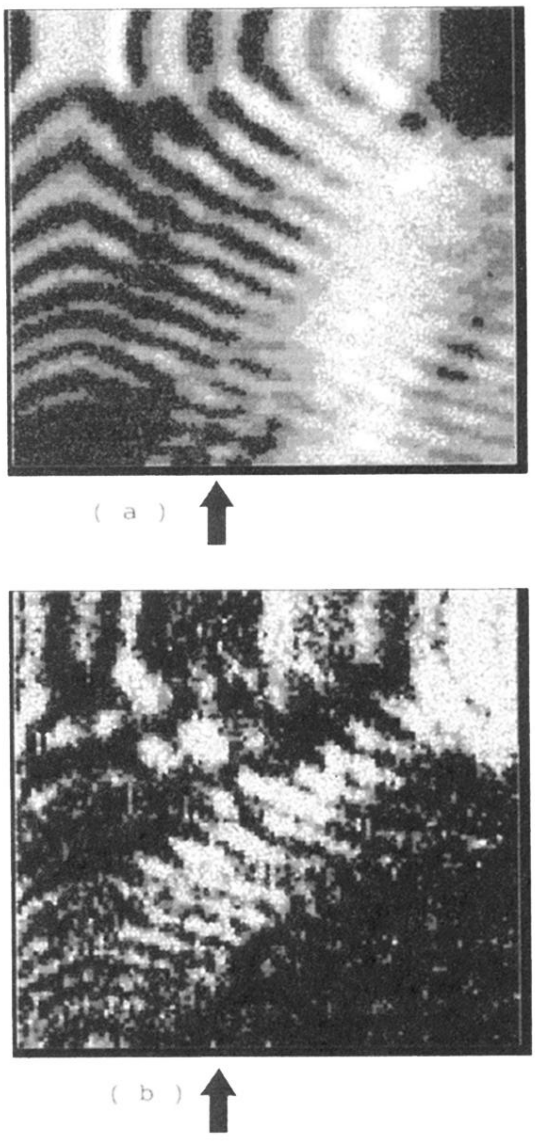

FIG. 9. Near-field optical images of $4\times4\ \mu m^2$ taken at nearly the same place as those in Fig. 7, and generated due to the fast (a) and slow (b) polaritons being resonantly excited in turn. The optical images are presented in different scales corresponding to $\sim$10–600 pW (a) and $\sim$0–30 pW (b) of the detected optical signal. Arrows indicate the directions of the cross sections shown in Fig. 10.